

Quantification of partial volume effects in planar imaging

Mpumelelo Nyathi¹, Enoch Sithole², Ouma Ramafi³

¹Department of Medical Physics, Faculty of Health Sciences, SMU, Pretoria, South Africa

²Department of Physics, Faculty of Pre-Clinical Sciences, SMU, Pretoria, South Africa

³Department of Nuclear Medicine, Dr. George Mukhari Academic Hospital, Pretoria, South Africa

(Received 4 September 2015, Revised 4 January 2016, Accepted 11 January 2016)

ABSTRACT

Introduction: The limited resolution of the imaging system causes partial volume effects (PVEs). These results in spreading of image counts to the neighboring pixels. This phenomenon is called spill-out effect. This study aimed at quantifying PVEs using ImageJ.

Methods: Technetium-99m solution of concentration of 74 kBq/ml was filled into spheres *A*, *B* and *C* of diameters: 26 mm, 20 mm and 16 mm respectively. The spheres were imaged mounted inside a Jaszczak phantom filled with activity free water using a Siemens E-Cam dual head gamma camera. Images were quantified using ImageJ following a two-step method. Step 1: Drawing of region of interest 1 (ROI 1) closely on the boundary of the planar image to extract images counts before PVEs correction. Step 2: Drawing region of interest 2 (ROI 2) to extract true sphere image counts. ROI 2 extends from the boundary of ROI 1 by the FWHM of the imaging system.

Results: The study revealed that PVEs are aggravated by decrease in sphere size. Underestimation of image counts on the 64×64 pixels matrix was found to be: 9.7%; 15% and 26% in the order of decreasing sphere size. However, an improvement in the spatial resolution decreased PVEs (128×128 pixels: 6.7%; 12.0% and 22.5%; 256×256 pixels: 6.5% ; 9% and 19.3%; 256×256 pixels: 6.1%; 8.0% and 18.7% in the order of decreasing sphere size).

Conclusion: ImageJ successfully quantified PVEs attributed to the spill-out effect in planar imaging.

Key words: Planar imaging; Partial volume effects; Quantification

Iran J Nucl Med 2016;24(2):115-120

Published: July, 2016

<http://irjnm.tums.ac.ir>

Corresponding author: Mpumelelo Nyathi, Box 672, 0204, Medunsa, South Africa. E-mail: mpumelelo.nyathi@smu.ac.za

INTRODUCTION

Quantitative nuclear medicine imaging facilitates determination of values for localized radioactivity concentrations in targeted organs [1-3]. The quantitative numerical values from the nuclear medicine images are used to infer on the physiological functions of the organs for successful implementation of diagnostic and therapeutic decisions [1-4]. However, the limited spatial resolution of the imaging system hinders accurate quantification. Activity concentrations are either underestimated or overestimated in organs with dimensions that are less than three times the full width half maximum (FWHM) of the imaging system's point spread function (PSF). This phenomenon is called partial volume effects (PVEs) [1-6]. It can result in spreading of activity outside the organ (spill-out effect) or contribution of activity from the neighboring organs to the targeted organ (spill-in effect) [7-9].

Spill-out effects may occur on their own in the absence of background activity. However both effects may occur simultaneously in the presence of a radioactive background. The background can either be the neighboring organs or blood pool in case of a patient [2]. The current study addresses only the impact of spill-out effects. These as mention earlier results in "loss" of activity from the organ or structure of interest resulting in apparent decrease of activity [2, 9]. Activity counts blur into the background [2, 9-11]. PVEs compromise accurate quantification of radiotracer distribution in targeted organs or structures [1, 2, 9-12].

In medical imaging PVEs are a common occurrence in brain and tumor imaging. They manifests as spill-out effects whereby the radioactivity blurs into the surrounding tissue from the brain cortex or tumor walls both of which are high activity regions leading to underestimation of tracer uptakes [10, 11]. Pretorius et al. observed considerable spill out of activity from the liver to the nearby heart wall [11]. They interpreted the process as a manifestation of PVEs in form of spill-out effect [11].

PVEs also manifest during quantification of the radiotracer distribution in tissue. An improvement in the ability to quantify activity in tissue is mandatory to oncologist. Most cancer therapies despite being effective are unacceptably toxicity to health tissues. Accurate quantification of a radiotracer absorption sheds light into tissue toxicity [13]. Informed decisions on whether to continue or discontinue treatment on grounds of tissue toxicity relies on ability to extract accurate quantitative values from nuclear medicine images. Accurate quantitative values of ^{99m}Tc accumulated in the parotid and submandibular glands via quantification of their

planar images can be used to infer to the degree of their damage post radiation therapy.

In this study we report on a procedure that was successfully implemented to quantify PVEs using ImageJ software aimed at recovery of image counts attributed to the spill-out effect on planar images of spheres of diameters: 26 mm, 20 mm and 16 mm.

METHODS

A Siemens E-Cam dual head gamma camera with detectors mounted with low energy high resolution collimators and linked to a Saturn nuclear medicine computer was used for data collection. The energy window was fixed at $140 \text{ keV} \pm 15\%$ photopeak. This $\pm 15\%$ photo peak window was found to be more efficient in rejecting Compton scatter photons compared to $\pm 20\%$ recommended in literature. The activity was assayed using a dose calibrator, Model PTW 4 Curiementor.

Preparation of activity concentration

The activity of ^{99m}Tc required to prepare ^{99m}Tc solution of concentration 74 kBq/ml was eluted from the vial using a syringe fitted with a needle. The syringe was assayed without the needle. The ^{99m}Tc activity was transferred from the syringe into the beaker where the targeted activity concentration was prepared.

The residual activity remaining in the syringed was also assayed. The value of the activity transferred into the beaker was obtained by subtracting residual activity from the activity of the syringe measured without the needle. The targeted concentration (74 kBq/ml) was prepared by uniformly mixing distilled water and ^{99m}Tc activity based on the following formula:

$$c = A/V \quad (1)$$

Where:

c: is the targeted activity concentration per millimeter of the required solution measured in Becquerel per milliliter.

A: is the activity of ^{99m}Tc measured in Becquerel using a dose calibrator

V: is the volume of distilled water, required to make the required concentration, measured in milliliters.

Preparation of phantom

A solution of activity concentration 74 kBq/ml was prepared in a beaker following instructions given in section 2.1. The solution (74 kBq/ml) was then filled into the spheres *A*, *B* and *C*. The spheres were then mounted inside the Jaszczak phantom using supporting rods (stems) as shown in Figure 1.

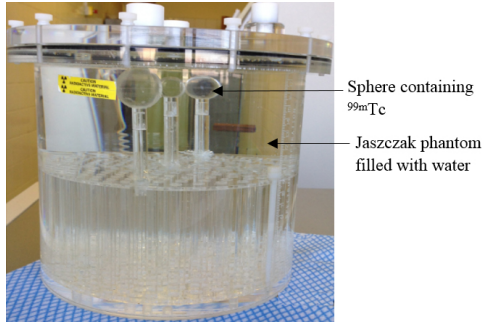


Fig 1. Lateral view of a Jaszczak phantom filled with water showing spheres mounted inside.

The Jaszczak phantom was then filled with activity free water and then placed on supine position on the gantry of the Siemens E-Cam dual head gamma camera ready for planar imaging.

Image acquisition

The Jaszczak phantom was imaged following a thyroid protocol used at Dr George Mukhari Academic Hospital. The protocol allows the use of one detector. Detector 1 which was positioned vertically above the Jaszczak leaving a distance of 5 cm between itself and the surface of the Jaszczak phantom was used. This distance gave the best spatial resolution without the detector having to touch the phantom. A set of five planar images of the three spheres were acquired on the following matrix sizes:

64 × 64 pixels; 128 × 128 pixels; 256 × 256 pixels; 512 × 512 pixels and 1024 × 1024 pixels. The duration of scanning was 5 minutes on each matrix size. Acquired events were processed into images using esoft software installed into a computer interfaced with the Siemens E-Cam dual head gamma camera.

Convention of image counts into activity

The activity concentration per ml (C) for the first image was calculated based on the formula:

$$C = \left[\frac{C_{image}}{V_{sphere}} \right] / t_{scan} \quad (2)$$

Table 1: Proportions of ^{99m}Tc and distilled water used to prepare a concentration of 74 kBq/ml.

Activity of ^{99m}Tc inside the syringe without needle (MBq)	Quantity of ^{99m}Tc used (MBq)	Residual activity (MBq)	Volume of distilled water used (ml)	Concentration of ^{99m}Tc solution prepared (kBq/ml)
27.69	27.64	0.05	373	74

Where:

C: is the targeted activity concentration per ml

C_{image} : is the counts in the desired region of interests

V_{sphere} : is the volume of sphere measured in ml

T_{scan} : scan duration

In calculating the activity concentration for the subsequent images, a decay correction factor (D) was applied. The formula for the decay correction factor is:

$$D = 0.5^{\frac{\Delta t}{t_{1/2}}} \quad (3)$$

Where:

Δt : is the time difference between scan time for the first image and the image in consideration expressed in hours

$t_{1/2}$: is the half-life of

The activity concentration per ml for subsequent images was calculated by the formulae:

$$C = \left(\frac{C_{image}}{V_{sphere}} \right) / t_{scan} \times [D] \quad (4)$$

RESULTS

Activity concentration

The column named residual activity in Table 1 (column 3) was the activity that remained in the syringe after emptying the assayed activity (column 1) into the beaker. Actual activity (column 2) was the activity used, it was obtained by subtracting residual activity from the activity in column 1. Column 5 shows the concentration of ^{99m}Tc solution that was prepared for use in this study.

Schematic representation of the PVEs

Figure 2 shows the planar images of the spheres A, B and C. The images appear blurred due to the spreading of images counts to the neighboring image pixels. This phenomenon is called partial volume effect, in this case study it manifested as spill-out.

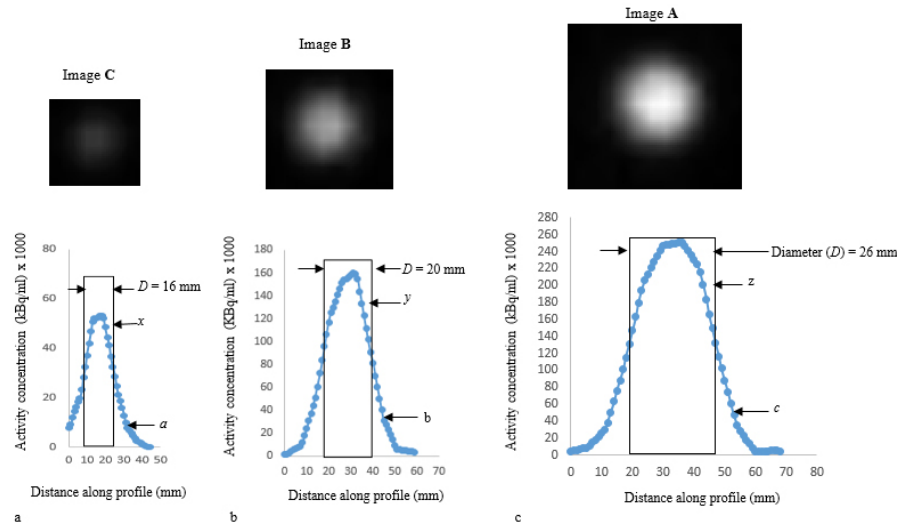


Fig 2. The planar images of the spheres *A*, *B* and *C*.

Below each planar image are corresponding activity profiles. Ideally the activity profiles should be rectangular in shape as shown in diagrams a, b and c (labelled *x*, *y* and *z*) respectively. However, due to the spill-out effect, the activity profiles are Gaussian functions represented by the curves *a*, *b* and *c*. The symbol *D* represents the diameter of the sphere. The pixel size of the images is 4.8 mm and the FWHM of the Siemens E-Cam dual head gamma camera at 5 cm distance from the collimator was 7.4 mm.

Image quantification software and quantification

ImageJ software was used to quantify all acquired planar images. ImageJ is characterized by a small economic window consisting of several usable tools. The circular tool was used as shown in Figure 3 to draw regions of interest needed for quantification of planar images in this study.

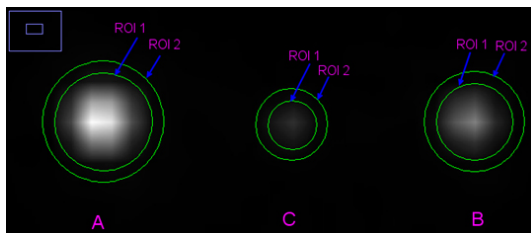


Fig 3. ROI 1 and ROI 2 drawn on planar images the spheres. ROI image counts are not a true reflection of the individual sphere image counts. It excludes image counts that have been displaced from the image due to spill-out effect. ROI 2, added on each planar image of sphere extracts true sphere image counts (this includes counts that were spread to the neighboring pixels due to spill-out effect). ROI 2 extends from the boundary of the image by the FWHM of the imaging system.

In Figure 3, the difference between image counts in ROI 2 and ROI 1 gives the image counts smeared on the neighboring pixels of the planar image. The smeared counts are responsible for underestimation of the regional distribution of activity in the spheres.

Image counts pre and post PVE correction extracted from planar image

Table 2 shows the image counts extracted from planar images of spheres *A*, *B* and *C*.

DISCUSSION

Quantification of PVEs

The results (Table 2) established that ImageJ can be successfully used to quantify PVEs in planar imaging. The differences between the images counts from ROI 2 and ROI 1 gave the image counts that were spread to the neighboring pixels of each of the three spheres (*A*, *B* and *C*). The spill-out effect was responsible for the spread of the image counts outside the image pixels. It was also observed that the spreading of image counts to the neighboring pixels contributed to the fuzzy appearance of the planar images of the spheres shown in Figure 2 (top images).

The fuzziness of the planar images (Figure 2) was attributed to apparent decrease of the regional distribution of activity inside the spheres. Image counts of the spheres were underestimated as was the true signal intensity inside the spheres. If spatial resolution of the imaging system was not limited, then the activity profile for the spheres should have been rectangular in shape as shown in Figure 2a, b and c (labelled *x*, *y* and *z*).

Table 2: The image counts extracted from planar images of spheres *A*, *B* and *C*.

Matrix size (pixels)	Name of sphere	Activity concentration inside the sphere 74 kBq/ml			
		ROI 1 counts	ROI 2 counts (A)	Recovered counts (B)	% Underestimation = B/A × 100
64 × 64	<i>A</i>	192949	213875	20926	9.7
	<i>B</i>	65258	76903	11645	15.0
	<i>C</i>	15325	20711	5386	26.0
128 × 128	<i>A</i>	174021	186517	12496	6.7
	<i>B</i>	62539	72392	8688	12.0
	<i>C</i>	14421	18615	4194	22.5
256 × 256	<i>A</i>	163158	174629	11471	6.5
	<i>B</i>	56743	62354	5611	9.0
	<i>C</i>	12875	15959	3084	19.3
512 × 512	<i>A</i>	128 516	136 814	8298	6.1
	<i>B</i>	49499	53801	4302	8.0
	<i>C</i>	10797	13277	2480	18.7
1024 × 1024	<i>A</i>	76273	82069	4760	5.8
	<i>B</i>	26264	28547	2283	7.9
	<i>C</i>	6094	7446	1352	18.2

However, due to the spill-out effect the activity profiles for the three spheres were found to be Gaussian curves (labelled *a*, *b* and *c*) in Figure 2a, b and c. The use of ImageJ facilitated recovery of these image counts that caused underestimation of image counts for the sphere. The recovered image counts for the respective spheres are presented in Table 2. They corresponds to the activity between the Gaussian functions *a*, *b* and *c* and rectangular profiles *x*, *y* and *z* for the respective spheres.

The study revealed that impact of spill-out effect is dependent on the object size and the spatial resolution. It can be observed that as sphere sizes decreased in the order *A*, *B* and *C*, the percentage error in underestimation of images counts also increased as follows 9.7%; 15% and 26% in the order of decreasing sphere size for images acquired on the 64× 64 pixels matrix size. However, as the spatial resolution was improved, the magnitude of the percentage error in quantification of PVEs decreased (128 × 128 pixels: 6.7%; 12.0% and 22.5%; 256 × 256 pixels: 6.5%; 9% and 19.3%; 512 × 512 pixels: 6.1%; 8.0% and 18.7%; 1024 × 1024 pixels: 5.8%; 7.9% and 18.2%) in the order of decreasing sphere size. Although it is true that increasing the spatial resolution reduces the PVEs, the authors found in the extended unpublished work yet another limitation with increase of matrix size. It introduced image noise as a result of decrease of the number of photons per pixel.

The matrix size of 128 × 128 pixels was found to successfully trade-off between image degradation caused by image noise and improvement of spatial

resolution. A matrix size of 128 × 128 pixels therefore successfully reduces PVEs and improves quantitative results in planar imaging. However the percentage error will increase with decrease in size of organ of interest. This implies that for large organs a quantification error as low as 6.7% can be obtained and for smaller organs of the dimensions similar to sphere *C*, it can be in the region of 22.5%. Activity quantification of large organs can be acceptable without having to bother about PVEs whereas for smaller organs such as salivary glands or tumors PVEs have to be taken into account. Introduction of PVEs correction would therefore be obligatory in order to improve quantification of activity in structures with dimensions that are less than the FWHM of the imaging system.

Comparison to other methods

One of the main advantages of the method used in this study is its successful extension to SPECT images reconstructed using FBP under implementation of a Butterworth filter using as filtering parameters a cut-off frequency of 0.9 and an order of 9. The use of this method and its flexibility for further extension to SPECT therefore makes it unique especially current methods for quantification used in SPECT were originally designed for PET imaging. The use of methods originally designed for PET in SPECT cannot be expected to give good estimates of the magnitude of PVEs since the PSF in PET is assumed invariant yet in SPECT it varies with the distance from the collimator

Furthermore, the method used in this study is cost effective, it uses a license free software. Other methods [12, 14], used require use of additional anatomical information on imaged structures [12, 14, 15] and others require use of coefficient recovery techniques [15]. The use of additional anatomical information based on high resolution MRI or CT images is a huge expense in routine clinical. The disadvantage of methods requiring use of recovery coefficients is that they require knowledge of the volume of the structures.

CONCLUSION

ImageJ successfully recovers the image counts that are responsible for underestimation of image counts from spheres *A*, *B* and *C* with dimensions less than 2-3 times the FWHM of the imaging system. These PVEs are size-dependent, the smaller the organ of interest the more pronounced will be the underestimates of signal intensity or acquired image counts in planar images hence the need of quantifying the PVEs. In medical imaging dealing with PVEs should be prioritized where informed decisions on diagnostic and therapeutic process are to be implemented.

REFERENCES

1. Buvat I. Quantification in emission tomography: challenges, solution, and performance. *Nucl Instrum Meth A*. 2007;571:10-13.
2. Erlandsson K, Buvat I, Pretorius PH, Thomas BA, Hutton BF. A review of partial volume correction techniques for emission tomography and their applications in neurology, cardiology and oncology. *Phys Med Biol*. 2012 Nov 7;57(21):R119-59.
3. Hofheinz F, Dittrich S, Pötzsch C, Hoff Jv. Effects of cold sphere walls in PET phantom measurements on the volume reproducing threshold. *Phys Med Biol*. 2010 Feb 21;55(4):1099-113.
4. Kirov AS, Pia JZ, Schmidlein CR. Partial volume correction in PET using iterative deconvolution with variance control based on local topology. Available from: <http://www.iop.org/EJ/abstract/0031-9155/53/10/009>. [cited 2015 Dec 1]
5. Teo BK, Seo Y, Bacharach SL, Carrasquillo JA, Libutti SK, Shukla H, Hasegawa BH, Hawkins RA, Franc BL. Partial-volume correction in PET: validation of an iterative postreconstruction method with phantom and patient data. *J Nucl Med*. 2007 May;48(5):802-10.
6. Strul D, Bendriem B. Robustness of anatomically guided pixel-by-pixel algorithms for partial volume effect correction in positron emission tomography. *J Cereb Blood Flow Metab*. 1999 May;19(5):547-59.
7. Hoetjes NJ, van Velden FH, Hoekstra OS, Hoekstra CJ, Krak NC, Lammertsma AA, Boellaard R. Partial volume correction strategies for quantitative FDG PET in oncology. *Eur J Nucl Med Mol Imaging*. 2010 Aug;37(9):1679-87.
8. Soret M, Bacharach SL, Buvat I. Partial-volume effect in PET tumor imaging. *J Nucl Med*. 2007 Jun;48(6):932-45.
9. Erlandsson K, Thomas B, Dickson Hutton BF. Partial Volume correction in SPECT reconstruction with OSEM. *Nucl Instrum Methods*. 2011;646:S85-S88 .
10. Du Y, Madar I, Stumpf MJ, Rong X, Fung GS, Frey EC. Compensation for spill-in and spill-out partial volume effects in cardiac PET imaging. *J Nucl Cardiol*. 2013 Feb;20(1):84-98.
11. Pretorius PH, King MA. Diminishing the impact of the partial volume effect in cardiac SPECT perfusion imaging. *Med Phys*. 2009 Jan;36(1):105-15.
12. Rosset OG, Zaidi H. Correction of Partial Volume effects in Emission Tomography. In: Zaidi H. Quantitative analysis in nuclear medicine imaging. New York: Springer Science Business Media, Inc.; 2006. p.237-265.
13. Green AJ, Dewhurst SE, Begent RH, Bagshawe KD, Riggs SJ. Accurate quantification of 131I distribution by gamma camera imaging. *Eur J Nucl Med*. 1990;16(4-6):361-5.
14. Ritt P, Vija H, Hornegger J, Kuwert T. Absolute quantification in SPECT. *Eur J Nucl Med Mol Imaging*. 2011 May;38 Suppl 1:S69-77.
15. Pereira JM1, Stabin MG, Lima FR, Guimarães MI, Forrester JW. Image quantification for radiation dose calculations--limitations and uncertainties. *Health Phys*. 2010 Nov;99(5):688-701.